Published in final edited form as:
Nano Lett. 2012 August 8; 12(8): 4131–4139. doi:10.1021/nl301658q.

Tracking Mesenchymal Stem Cells with Iron Oxide Nanoparticle Loaded Poly(lactide-co-glycolide) Microparticles

Chenjie Xu[1], **David Miranda-Nieves**[1], **James A. Ankrum**[1], **Mads Emil Matthiesen**[1], **Joseph A. Phillips**[1], **Isaac Roes**[1], **Gregory R. Wojtkiewicz**[2], **Vikram Juneja**[1], **Jens Roat Kultima**[1,4], **Weian Zhao**[1], **Praveen Kumar Vemula**[1], **Charles P. Lin**[3], **Matthias Nahrendorf**[2], and **Jeffrey M. Karp**[1,*]

[1]Division of Biomedical Engineering, Department of Medicine, Center for Regenerative Therapeutics, Brigham and Women's Hospital, Harvard Medical School, Harvard Stem Cell Institute, Harvard-MIT, Division of Health Sciences and Technology, 65 Landsdowne Street, Cambridge, MA 02139

[2]Center for Systems Biology, Massachusetts General Hospital, and Harvard Medical School, Boston, Massachusetts 02114

[3]Advanced microscopy program, Center for Systems Biology and Wellman Center for Photomedicine, Massachusetts General Hospital, Harvard Medical School, Boston, Massachusetts 02114

[4]EMBL, Meyerhofstrasse 1, 69117 Heidelberg, Germany

Abstract

Monitoring the location, distribution and long-term engraftment of administered cells is critical for demonstrating the success of a cell therapy. Among available imaging-based cell tracking tools, magnetic resonance imaging (MRI) is advantageous due to its non-invasiveness, deep penetration, and high spatial resolution. While tracking cells in pre-clinical models via internalized MRI contrast agents (iron oxide nanoparticles, IO-NPs) is a widely used method, IO-NPs suffer from low iron content per particle, low uptake in non-phagocytotic cell types (e.g., mesenchymal stem cells, MSCs), weak negative contrast, and decreased MRI signal due to cell proliferation and cellular exocytosis. Herein, we demonstrate that internalization of IO-NP (10 nm) loaded biodegradable poly(lactide-co-glycolide) microparticles (IO:PLGA-MPs, 0.4–3μm) in MSCs enhances MR parameters such as the r_2 relaxivity (5-fold), residence time inside the cells (3-fold) and R_2 signal (2-fold) compared to IO-NPs alone. Intriguingly, *in vitro* and *in vivo* experiments demonstrate that internalization of IO:PLGA-MPs in MSCs did not compromise inherent cell properties such as viability, proliferation, migration and their ability to home to sites of inflammation.

Introduction

Mesenchymal stem cells (or multipotent stromal cells, MSCs) hold great promise for the treatment of multiple diseases and disorders including graft versus host disease[1], type I diabetes[2], and myocardial infarction[3]. To develop effective MSC therapies, it is essential in

*Correspondence should be addressed to JMK (jkarp@rics.bwh.harvard.edu).

Competing Financial Interests

J.M.K. is a co-owner of Megacell Therapeutics, a company that has an option to license IP generated by J.M.K. J.M.K. may benefit financially if the IP is licensed and further validated. The interests of J.M.K. were reviewed and are subject to a management plan overseen by the Brigham & Women's Hospital and Partners HealthCare in accordance with their conflict of interest policies. The remaining authors declare no competing financial interests.

both experimental models and clinical trials to monitor and understand the location, distribution and long-term engraftment of administrated cells, preferably in a noninvasive manner. This will facilitate evaluation of treatment efficacy; reveal optimal transplantation conditions including cell dosage, delivery route, timing of injections; and ultimately improve patient treatment[4].

Recently, imaging techniques including optical imaging, radionuclide imaging and magnetic resonance imaging (MRI), have been used for tracking transplanted MSCs[4b, 5]. However, they suffer from limitations. For example, optical imaging is limited by the penetration ability of light, and radionuclide imaging suffers from the poor spatial resolution and rapid decay of radioisotopes[6]. In comparison, MRI is an attractive tool for longitudinal MSC monitoring of specific tissue locations in humans because of its non-invasiveness, deep penetration, high spatial resolution (~100 μm) and the relatively longer retention of MRI contrast agents in cells[7].

Currently, the most widely used labeling agents for MRI tracking are iron oxide (Fe_3O_4) nanoparticles (IO-NPs) with core size ranging from 4 nm to 20 nm[8]. Despite their favorable biocompatibility, IO-NPs suffer from time-dependent decrease in MRI signal due to cell proliferation and exocytosis of IO-NPs9. When a cell proliferates, particles (either NPs or MPs) are distributed evenly or unevenly between two daughter cells. After a few cycles, only a fraction of cells contain particles and become undetectable. However, if the signal from a single particle was strong enough to be detected by MRI (e.g., polystyrene-based microparticles6), those cells containing one or more particles should be detectable. Furthermore, exocytosis dilutes particle concentration10. Interestingly, the exocytosis process is dependent on particle size11; bigger particles are exocytosed at a slower rate. Previously we have shown that MSCs can efficiently internalize 1–2 micron sized biodegradable poly(lactide-co-glycolide) microparticles (PLGA MPs) that are loaded with differentiation factors, and the particles remain localized within the cell for several days12. Combining these two ideas, we hypothesized that a micron-sized particle with stronger MRI signal and reduced exocytosis could address the dilution limitation of IO-NPs and enable the longitudinal tracking of MSCs.

Herein, we demonstrate that confinement of IO-NPs in micron-sized PLGA particles (IO:PLGA-MPs) both enhances molar relaxivity of the Fe and localization (through concentrating Fe in discreet locations) that increases the signal to noise ratio, and leads to longer detectable time of labeled MSCs compared to IO-NPs. Furthermore, the effects of IO:PLGA-MPs on MSC viability, proliferation, migration, and cell homing ability have been investigated using a series of *in vitro* and *in vivo* models.

Results and discussion

1. Design of IO-NP encapsulated PLGA MPs for cell labeling

To evaluate the effect of size on particle retention time in cells, we labeled MSCs with either fluorescent polystyrene NPs (50 nm) or polystyrene MPs (1 μm) (Bangs Labs). Subsequently, fluorescent intensity of the labeled MSCs was monitored over two weeks using flow cytometry (SI Figure 1). When MSCs were labeled with NPs, fluorescent-positive MSCs constituted 80% and 10% at day-1 and day-7, respectively. On the contrary, at day-1 and day-7, 100% and 70% of the microparticle labeled MSCs demonstrated positive fluorescent signals. After 14 days, only microparticle-labeled cells showed fluorescence (>30% of the cells). This suggests that micron-sized particles are retained within cells for the long term, which should permit prolonged cell tracking. Thus, we further explored encapsulation of IO-NPs in biocompatible and biodegradable PLGA MPs that can be

internalized by cells as a potential strategy to improve cell labeling with MRI contrast agents.

2. Fabrication and characterization of IO:PLGA-MPs

A schematic of the IO:PLGA-MPs fabrication method is described in Figure 1A. Oleic acid stabilized IO-NPs (10 nm core size and 25 nm hydrodynamic diameter, SI Figure 2)[13] were encapsulated in PLGA (inherent viscosity: 0.55–0.75 dL/g with carboxyl end-groups) using a single emulsion method[9a]. Scanning and transmission electron microscope images (SEM and TEM, respectively) show that IO:PLGA-MPs were spherical in shape an average size ~0.8μm (SEM, Figure 1B, and SI Figure 2), and IO-NPs were encapsulated within the core of PLGA-MPs (TEM, Figure 1C). The amount of Fe loading was quantified using Inductively Coupled Plasma Atomic Emission Spectroscopy (ICP-AES) after the dissolution of IO PLGA-MPs in 70% nitric acid. The IO:PLGA-MPs had Fe loading of 15.65±1.2 wt% (Fe_3O_4 weight percentage of 21.61±1.7%). IO-NPs functionalized with carboxy groups were utilized as a control for all experiments.

Magnetic properties of IO:PLGA-MPs were studied by a vibration sample magnetometer (VSM) (Figure 2A). The saturation magnetization (*Ms*) values of IO-NPs and IO:PLGA-MPs were found to be ~ 40 emu/gram of iron, which is consistent with previous reports[14]. The hysteresis curve of IO:PLGA-MPs matches well with that of IO-NPs, which indicates that encapsulation did not change the inherent superparamagnetic property of IO-NPs. The magnetic properties were further examined with T_2 relaxation rate ($1/T_2$) as a function of iron concentration by a benchtop magnetic resonance relaxometer (Figure 2B). The magnetic relaxivity (r_2) values were derived from the slope of the linear fit, which revealed that the encapsulation of IO-NPs in PLGA matrix significantly increased r_2 from 61.16 to 316.6 $mM^{-1}{\cdot}s^{-1}$ (~5-fold) compared to IO-NPs, which was the result of IO-NP aggregation inside PLGA and thus their enhanced ability to decrease the transverse relaxation time of protons in surrounding water 9a, 15. The increased magnetic relaxivity enhances the hypointense signal. As shown in Figure 2C, when dispersed in a 3% agarose hydrogel suspension, IO:PLGA-MPs provided higher negative contrast (higher $1/T_2$ or R_2 value) than IO-NPs, as suggested by the pseudocolor in Figure 2C. The average R2 signal from IO:PLGA-MPs was approximately twice that of the signal generated from IO-NPs.

To examine the potential for enhanced contrast of IO:PLGA-MPs *in vivo*, suspensions of both IO-NPs and IO:PLGA-MPs in agarose gels (without cells) were injected subcutaneously into the back of a healthy mouse (Figure 3A). 60 minutes after injection, the mouse was subjected to whole body multi-slice multi-echo T_2 weighted MRI. The collected images were reconstructed into a 3D $1/T_2$ (R_2) volumetric image (Figure 3B) through Amira-Visage Imaging software. Pseudocolor was applied to reveal the contrast enhancement of particles. As shown in Figure 3B, IO:PLGA-MPs generated a stronger negative contrast than IO-NPs using two Fe concentrations (20 μg Fe/ml (0.36mM) and 40 μg Fe/ml (0.71mM)). Under both conditions, the average R_2 signal from IO:PLGA-MPs was approximately twice that of the signal generated from IO-NPs.

3. Labeling MSCs with IO:PLGA-MPs

Given that positively charged particles typically show enhanced internalization into the cells compared to negatively charged particles[16], the negatively charged IO-NPs and MP, as measured by zeta potential (−30±10mV and −2.7±1.0mV in PBS accordingly), were coated with poly-L-lysine coating leading to a surface charge of 10±5.2mV and 15.1±6.2 mV in PBS. To remove potential signal from free particles, typically, IO:PLGA-MPs were incubated with MSCs for 12 hours at physiological conditions, and then cells were detached by trypsinization and purified from free particles with Ficoll-Paque.[17]

Particles were applied to cells while maintaining a constant Fe concentration (25, 50, 100 or 200 μg/mL) and the amount of Fe loaded into the cells was quantified. This was achieved by digesting the cells and quantifying the Fe content via ICP-AES. The maximum Fe loading/cell was attained at 100μg/mL initial concentration (Figure 4A). Further increases in the initial Fe concentration did not enhance the final quantity of Fe per cell. Interestingly, maximal Fe loading per cell was 20 and 80 pg Fe/cell for IO-NPs and IO:PLGA-MPs, respectively. A significant 4-fold increase for Fe loading per cell reveals the advantage of using MPs for internalization of iron oxide. Given that no statistically significant difference was found in Fe loading between 50–100 μg/mL, to minimize use of reagents further internalization experiments were performed using 50 μg/mL of Fe.

To assess changes in Fe content over time, following particle internalization and subsequent purification from free particles, MSCs were plated in T25 plates for 28 days (the labeling day was designated as day 1). The culture media was replaced every two days for all samples and at each time point (day 1, 2, 4, 6, 12, and 28) MSCs were collected for quantification of MSC the proliferation, Fe concentration, and MRI analysis (by dispersing 200,000 MSCs in 1mL 3% agarose gel). As shown in Figure 4B, when MSCs were labeled with IO-NPs, the iron concentration per MSC decreased to about half of the initial value after 4 days. The iron concentration per cell was close to background after 12 days, however, when MSCs were labeled with IO:PLGA-MPs, within 6 days the concentration had decreased to half of its initial value and after 25 days, the iron concentration per cell was still significantly higher than background. The combination of contrast enhancement, and increased cellular loading in MSCs of IO:PLGA-MPs permitted us to visualize MSCs with MRI for at least 12 days (Figure 4C), while in the case of IO-NPs labeling there was minimal detectable signal after day 6. To further confirm the MRI results and examine the stability of the internalized IO:PLGA-MPs, we labeled MSCs with fluorescent IO:PLGA-MPs containing lipophilic carbocyanine dye (i.e. DiI), and examined the fluorescent signal with fluorescent confocal microscopy. 18 days after labeling, we still observed the presence of IO:PLGA-MPs in 15±5% MSCs (Figure 4D), which revealed the potential of IO:PLGA-MPs for the long-term tracking of MSCs.

The location of internalized IO:PLGA-MPs and IO-NPs in MSCs after 12 hours labeling was characterized using TEM. In both cases, particles were present in intracellular compartments (Figure 5). However, enhanced local density of IO-NPs was observed when they were encapsulated within PLGA-MPs (Figure 5A) whereas in the absence of PLGA-MPs, lower density of IO-NPs was observed in a scattered manner (Figure 5B). This result suggests that the advantage of IO-NPs encapsulation in PLGA-MPs may be enhanced contrast due to particle clustering[18].

4. IO:PLGA-MPs impact on MSCs

To investigate the potential negative impact on MSC phenotype, the viability, proliferation and migration ability of MSC were examined following IO:PLGA-MPs internalization using a series of *in vitro* and *in vivo* experiments. As shown in Figure 6A, there was no noticeable influence on cell viability for both types of magnetic particles compared to native cells 24 hours following particle internalization. To assess the potential impact on cell proliferation, MSCs were labeled with two types of magnetic particles and studied for 12 days (Figure 6B), during which confluence was reached typically at day 9. Compared with the control, MSCs labeled with both types of magnetic particles showed similar rates of proliferation. The number of MSCs tripled in 5 days.

The migration of MSCs *in vitro* was examined with a transwell assay. MSCs with or without internalized particles in media with 1% FBS were seeded on the insert, which was placed in chambers receiving complete media (with 10% FBS). MSCs with or without internalized

particles showed similar adhesion on the insert 1hr following cell seeding (SI Figure 3). Sixteen hours later, the migrated MSCs (bottom of filter) were stained and counted. Similar to Huang's report[19], MSC modified with IO-NPs showed a statistically significantly increased level of migration rate (~3x) (Figure 6C,D&F). The mechanism mediating this increase is not well understood. The encapsulation of IO-NPs inside PLGA limited this effect. MSCs labeled with IO:PLGA-MPs showed similar migration through the 8 μm membrane as the unlabeled MSCs (Figure 6C, E&F).

5. Homing of labeled MSCs in an inflamed ear model

The *in vitro* migration assay (Figure 6C–F) revealed that internalization of IO:PLGA-MPs does not impact MSC migration. Given that homing of systemically administered MSCs can be influenced by factors not accounted for in our *in vitro* assay including shear stress, immune system interference and endothelial barriers[20], we investigated the influence of internalized IO:PLGA-MPs on MSCs ability to home *in vivo* to a distant site of inflammation in an mouse model.

Previously, we examined the homing of systemically infused MSCs to a site of inflammation *in vivo* with dynamic real-time intravital confocal microscopy, using injection of lipo-polysaccharide (LPS) into the ear of a mouse[21]. To facilitate cell imaging, unlabeled MSCs and MSCs labeled with IO:PLGA-MPs (>97% labeling efficiency) were treated with cell tracker dyes (DiD, Molecular Probes) and infused via tail vein. After 24 hours, the ears were imaged with intravital confocal microscopy. As we have previously shown, unmodified MSCs preferentially migrate to inflamed sites (Figure 7A&B). Similarly, IO:PLGA-MPs labeled MSCs exhibited a similar response (Figure 7C&D). The number of cells at the site of inflammation was comparable between the IO:PLGA-MPs labeled and unlabeled MSCs. Approximately 20-fold more cells per unit volume were found in the inflamed ear (Figure 7E) compared to non-inflamed (saline) ear. In both cases, ~1/3 MSCs had transmigrated outside the blood vessel into the ear tissue, indicating that particle labeling did not impact transendothelial migration. Collectively, these results reveal that labeling of MSCs with IO:PLGA-MPs does not negatively impact MSC phenotype.

Conclusion

Herein, we demonstrated that MSC internalization of IO-NP (10 nm) loaded biodegradable MPs (0.8 μm) can enhance MR parameters such as the relaxivity (5-fold), residence time inside the cells (3-fold) and R_2 signal (2-fold) compared to free IO-NPs. Intriguingly, *in vitro* and *in vivo* experiments demonstrated that MSC internalization of IO:PLGA-MPs did not compromise inherent cell properties such as viability, proliferation, migration and their ability to systemically home to sites of inflammation. Thus, labeling cells with IO:PLGA-MPs may offer a potential opportunity for longitudinal tracking of MSC or other cell types without compromising cell phenotype including cell migration/homing ability.

Materials and Methods

All chemicals and solvents were of analytical grade from Sigma-Aldrich and were used without further purification unless otherwise mentioned. IO-NPs coated with oleic acid and water-soluble IO-NPs functionalized with carboxy groups were purchased from Ocean Nanotech (AR).

Mesenchymal stem cell culture and characterization

Primary human MSCs were obtained from the Texas A&M Health Science Center, College of Medicine, Institute for Regenerative Medicine at Scott & White Hospital, which has a

grant from NCRR of the NIH, Grant #P40RR017447. MSCs were derived from healthy consenting donors and thoroughly characterized as previously described.[22] MSCs were maintained in α-MEM expansion media (Invitrogen) supplemented with 15% Fetal Bovine Serum (Atlanta Biologicals), 1% (v/v) L-Glutamine (Invitrogen), and 1% penicillin:streptomycin solution (Invitrogen). Cells were cultured to 70–80% confluence before passaging. All experiments were performed using MSCs at passage number 3–6, where cells expressed high levels of MSC markers CD90 and CD29 (>99% cells), yet did not express hematopoietic markers CD34 or CD45 as observed from flow cytometry analysis. Before cell experiments, MSCs were detached with Trypsin 0.05% - EDTA 0.53mM (Gibco) and filtered with 40 μm Nylon Mesh (Fisher Scientific)..

Animal welfare

BALB/C mouse (Charles River Laboratories, Wilmington, MA) were used for the *in vivo* studies. All studies were in accordance with US National Institutes of Health guidelines for care and use of animals under approval of the Institutional Animal Care and Use Committees of Massachusetts General Hospital (Protocol number 2010N000064). All injections were performed under anesthesia, and all efforts were made to minimize suffering. Animals were humanely sacrificed after experiments.

Fabrication of IO:PLGA-MPs

Particles were prepared by following the procedures developed by Nkansah et al[14] with some minor modifications. Briefly, 10 mg Fe_3O_4 NPs (10 nm, Ocean Nanotech, AR) coated with oleic acid were mixed with 100 mg PLGA (acid terminated, 50:50, I.V.: 0.55–0.75 dL/g, Durect® Absorbables Durect Corporation) in 2 mL chloroform. The organic phase was then added to 20 mL of a 3% (w/v) aqueous solution of poly(vinyl alcohol) (MW: 90k, 80% hydrolyzed). To make the micronsized particles, a homogenizer (Tissue Master 125, Omni International) was used to disperse the organic phase into the aqueous phase (24,000 rpm for 2 min) in a 50 mL beaker. The homogenized mixture was then stirred overnight in a chemical fume hood at room temperature to allow for evaporation of chloroform. Finally, particles were isolated by centrifugation at 7,500 rpm for 5 minutes, washed thrice with distilled water, frozen at −80°C and lyophilized for 2 days.

Characterization of IO:PLGA-MPs

TEM—The IO:PLGA-MPs were subject to dehydration using graded ethanol (20%, 40%, 60%, 80%, 100%) and embedded in Epon 812 resin. Resin blocks were sectioned using a microtome and imaged with JEOL 200CX (80kV).

SEM—The IO:PLGA-MPs were deposited on silica wafers and coated with 10 nm gold. Then the PLGA-particle morphology was visualized via SEM (JEOL 6320 at 5kV).

Iron quantification—Iron content of particles was determined using ICP (HORIBA JOBINYVON, model: Activa) after digestion in 70 % nitric acid.

Hydrodynamic diameter quantification—The hydrodynamic diameter and polydispersity of particles were collected by Malvern Zetasizer Nano ZS90 in water by averaging 3 runs.

Hysteresis loop measurement—Samples were examined with a magnetometer (DMS Model 880 VSM vintage) at 37 °C. The measurements were normalized for the grams of iron in each sample, verified through ICP.

Relaxivity measurement *(r_2)* with benchtop relaxmeter—The Fe concentration of samples was quantified with ICP first. Then five solutions with different Fe concentrations were prepared and placed in NMR tubes. T2 was measured in the Minispec Mq-20 (Bruker Optik GmbH, Germany). r_2 was derived by extracting the slope from the plot of 1/T2 versus Fe concentration (mM).

Sample preparation for MRI—The particles were diluted to different concentrations (0, 5, 10, 15, 20, and 40 μg Fe/mL) in PBS and mixed with equivalent volume of 6% agarose-gel solution to obtain a final agarose concentration of 3%. Subsequently, the mixture was pipetted into a 3% agarose-gel-made plate. Pipetting was gently performed to avoid air bubbles. After 12 hours, MRI samples were imaged using a 4.7 T Bruker Pharmascan scanner at 37°C.

***In-vivo* MRI of IO:PLGA-MP—**A BALB/C mouse (Charles River Laboratories, Wilmington, MA) was used for the *in vivo* studies. Mice were anesthetized using ketamine/xylazine first. Then 45μL 3% agarose gels containing either IO-NPs or IO:PLGA-MPs with 20 and 40 μg Fe/ml were subcutaneously injected on the back of the mouse. After one hour the mice were euthanized and multi-slice multi-echo T2 (TR = 2800 ms, 4 averages, 128×128×16 matrix size, 0.432 mm × 0.312 mm × 1 mm voxel size) scanning was performed with effective echo times of 8.68, 17.36, 26.04, 34.72, 43.40, 52.08, 60.76, 69.44, 78.12, 86.80, 95.48, 104.16, 112.84, 121.52, 130.20, and 138.88 ms on the mouse with a 4.7 T Bruker Pharmascan scanner along with a RARE T2 sequence (TR= 2000 ms, effective TE = 36.0, 256×256×16 matrix size, 0.216 mm × 0.156 mm × 1 mm voxel size) ms, 8 averages). Amira (Visage Imaging) was used for the 3D reconstructions, which utilized the T2 maps calculated within the Osirix environment.

MSCs labeling with IO:PLGA-MPs

Particles were incubated with Poly-L-lysine (0.01%) for 40 minutes at room temperature in PBS. Then, the complex was added to cells in α-MEM expansion media supplemented with 1% FBS, 1% (v/v) L-Glutamine, and 1% penicillin:streptomycin solution for 12 hours. Cells were then permitted to recover in fresh media (15% FBS). For experimentation, labeled cells were washed twice with PBS, trypsinized, centrifuged with Ficoll-Paque (GE Healthcare), re-dispersed and counted in PBS. Labeling efficiency of MSCs with IO:PLGA-MPs: to facilitate the identification of particles internalized within MSCs, we incorporated the fluorescent dye, DiI during the preparation of IO:PLGA-MPs. Then MSCs were labeled with the fluorescent IO:PLGA-MPs and analyzed with flow cytometry.

Fe quantification in MSCs—For a typical sample, 0.1 mL of cell suspension was digested overnight using 0.3 mL concentrated nitric acid (~70%) and 0.1 mL hydrogen peroxide (30%). Samples were then diluted to a volume of 10 mL with deionized water, yielding a final nitric acid concentration of 2%. Iron concentration was determined with ICP.

MRI sample preparation—Agar wells were prepared using a 3% agar solution heated in a water bath until fully dissolved and poured into a PDMS mold. MSCs suspension samples were mixed with agar powder to a concentration of 3% and heated. Once the agar was fully dissolved, samples were transferred into an agar well and allowed to set. MRI samples were imaged using a Bruker 4.7 T MRI scanner.

TEM—MSCs were labeled with IO-NPs or IO:PLGA-MPs (50 μg Fe/mL) for 12 hours, and then washed twice with PBS. MSCs were fixed in phosphate-buffered Karnofsky's solution followed by staining with 2% osmium tetroxide at 4°C overnight, and dehydration using graded ethanol and embedded in Epon 812 resin. Resin blocks were sectioned using a

microtome, doubly stained with uranyl acetate and lead hydroxide, and imaged with JEOL 200CX (80kV).

Influence of magnetic particle labeling on MSC properties

Viability study—200,000 MSCs were seeded in T25 flasks 24 hours before the experiment. Poly-L-lysine coated IO-NPs or IO:PLGA-MPs dispersed in serum free media were added to the plates and incubated for 24 hours at 37°C. Unmodified MSCs were treated with serum free media in the same way. Then, the cells were permitted to recover in fresh media (15% FBS) for 30 minutes before being collected with 1X trypsin. Finally, the collected cells were counted. Each condition was performed in triplicate.

Proliferation assessment—2 million MSCs were labeled with magnetic particles (IO-NPs or IO:PLGA-MPs) as described above and sub-cultured in T25 flasks. At each time point (day 1, 3, 6, 9, 12), MSCs in three flasks were trypsinized and counted.

Transwell migration assay—In a 24- well transwell plate (FluoroBlok™ 8.0 μm colored PET membrane, BD), complete medium with 10% FBS was added into the (bottom) wells. 30,000 MSCs labeled with particles and purified with Ficoll-Paque were seeded into the insert in media containing 1% FBS. After 16 hours of incubation at 5% CO_2 and 37°C, inserts were washed twice with PBS, fixed in 4% paraformadehyde for 15 minutes, stained in 0.5% Phalloidin-FITC (Sigmal-Aldrich) for 10 minutes, and counted.

In-vivo MSC homing

Cell preparation—18 hours prior to injection, MSCs were labeled with IO:PLGA-MPs as described above. 2 hours before injection, serum-free medium was replaced with 15% FBS containing MEM-α for 30 min. Then cells were trypsinized, centrifuged, and re-suspended at 2×10^6 cells/mL in PBS. DiD stock (Invitrogen Inc.) was diluted to 20 μM in PBS. Equivalent volumes of cells and DiD solution were mixed together and incubated for 20 minutes at room temperature in the dark. Then, the labeled MSCs were centrifuged and washed twice with PBS. Finally, MSCs were passed through a 40μm cell strainer, and resuspended at 10^7 cell/mL in PBS.

Animals—BALB/C mice (Charles River Laboratories, Wilmington, MA) were anesthetized using ketamine/xylazine and the hair around the base of both ears was trimmed with scissors. To assess the potential for IO:PLGA-MP loaded MSCs to preferentially home to a site of inflammation, we utilized a model where 24 hours prior to cell infusion, inflammation was induced through injection of 30μg of E. coli lipopolysaccharide (LPS, Sigma, St. Louis, MO) in 30 μL of saline into the base of the left ear, whereas the right ear received 30μL 0.9% of saline as a control. 1×10^6 MSCs suspended in 100 μL PBS (pH 7.4) were injected retro-orbitally 24 hours post LPS injection. For delineation of vasculature during imaging, ~100 μL of 2 mg/mL FITC-dextran (2×10^6 kDa; Sigma, St. Louis, MO) was injected retro-orbitally just prior to imaging.

Dynamic real-time intravital confocal microscopy—Homing of unmodified and modified MSCs to the skin was imaged noninvasively (in real time) using a custom-built video-rate laser-scanning confocal microscope designed specifically for live animal imaging[23]. To image the vasculature and surrounding tissue, we positioned the mouse's ear on a coverslip (with index matching gels) and obtained high-resolution images with cellular details through the intact mouse skin at depths of up to 250 μm. The laser beams were focused onto the sample (mouse ear skin) using a 60X, 1.2NA water immersion objective lens (Olympus, Center Valley, PA). DiD-labeled MSCs were excited with a 635 nm continuous-wave (CW) laser (Coherent, Inc., Santa Clara, CA) and detected through a 695

nm ± 27.5 nm band pass filter (Omega Optical, Brattleboro, VT). FITC-dextran was excited with a 491 nm CW laser (Cobalt, Stockholm, Sweden) and detected through a 520 ± 20 nm bandpass filter (Semrock, Inc., Rochester, NY). For static images, 15 frames were averaged from the live video mode to improve the signal to noise ratio. The total number of "homed" cells from each MSC population within the mouse ear was quantified from the z-stacks acquired. For publication purposes, the contrast and brightness of the images were changed using ImageJ software.

Supplementary Material

Refer to Web version on PubMed Central for supplementary material.

Acknowledgments

This work was supported by the Harvard Stem Cell Institute, and the National Institute of Health grants HL095722 and HL097172 to JMK. D.M.N is supported by MIT-UROP program and the John Reed Fund. J.A.A. is supported by the Hugh Hampton Young Memorial Fund and the National Science Foundation. M.N. was supported by funds from the National Heart, Lung, and Blood Institute, National Institutes of Health, Department of Health and Human Services, under Contract No. HHSN268201000044C. We thank Dr. Nikolay Sergeyev (MGH) in "Center for Systems Biology Mouse Imaging Program" for helping us perform the relaxivity measurement with the benchtop relaxometer.

References

1. (a) Perez-Simon JA, Lopez-Villar O, Andreu EJ, Rifon J, Muntion S, Campelo MD, Sanchez-Guijo FM, Martinez C, Valcarcel D, del Canizo C. Mesenchymal stem cells expanded in vitro with human serum for the treatment of acute and chronic graft-versus-host disease: results of a phase I/II clinical trial. Haematol-Hematol J. 2011; 96(7):1072–1076.(b) Tian Y, Deng YB, Huang YJ, Wang Y. Bone marrow-derived mesenchymal stem cells decrease acute graft-versus-host disease after allogeneic hematopoietic stem cells transplantation. Immunol Invest. 2008; 37(1):29–42. [PubMed: 18214798]
2. (a) Fiorina P, Jurewicz M, Augello A, Vergani A, Dada S, La Rosa S, Selig M, Godwin J, Law K, Placidi C, Smith RN, Capella C, Rodig S, Adra CN, Atkinson M, Sayegh MH, Abdi R. Immunomodulatory Function of Bone Marrow-Derived Mesenchymal Stem Cells in Experimental Autoimmune Type 1 Diabetes. J Immunol. 2009; 183(2):993–1004. [PubMed: 19561093] (b) Ezquer FE, Ezquer ME, Parrau DB, Carpio D, Yanez AJ, Conget PA. Systemic administration of multipotent mesenchymal stromal cells reverts hyperglycemia and prevents nephropathy in type I diabetic mice. Biol Blood Marrow Tr. 2008; 14(6):631–640.
3. (a) Aggarwal S, Pittenger MF. Human mesenchymal stem cells modulate allogeneic immune cell responses. Blood. 2005; 105(4):1815–1822. [PubMed: 15494428] (b) Barbash IM, Chouraqui P, Baron J, Feinberg MS, Etzion S, Tessone A, Miller L, Guetta E, Zipori D, Kedes LH, Kloner RA, Leor J. Systemic delivery of bone marrow-derived mesenchymal stem cells to the infarcted myocardium - Feasibility, cell migration, and body distribution. Circulation. 2003; 108(7):863–868. [PubMed: 12900340]
4. (a) Lee Z, Dennis JE, Gerson SL. Imaging stem cell implant for cellular-based therapies. Exp Biol Med (Maywood). 2008; 233(8):930–40. [PubMed: 18480418] (b) Srinivas M, Aarntzen E, Bulte JWM, Oyen WJ, Heerschap A, de Vries IJM, Figdor CG. Imaging of cellular therapies. Adv Drug Deliv Rev. 2010; 62(11):1080–1093. [PubMed: 20800081]
5. Xu C, Mu L, Roes I, Miranda-Nieves D, Nahrendorf M, Ankrum JA, Zhao W, Karp JM. Nanoparticle-based monitoring of cell therapy. Nanotechnology. 2011; 22(49):494001. [PubMed: 22101191]
6. Stuckey DJ, Carr CA, Martin-Rendon E, Tyler DJ, Willmott C, Cassidy PJ, Hale SJM, Schneider JE, Tatton L, Harding SE, Radda GK, Watt S, Clarke K. Iron Particles for Noninvasive Monitoring of Bone Marrow Stromal Cell Engraftment into, and Isolation of Viable Engrafted Donor Cells from, the Heart. Stem Cells. 2006; 24(8):1968–1975. [PubMed: 16627684]
7. (a) Kraitchman DL, Bulte JWM. Imaging of stem cells using MRI. Basic Res Cardiol. 2008; 103(2): 105–113. [PubMed: 18324366] (b) Rogers WJ, Meyer CH, Kramer CM. Technology Insight: in

vivo cell tracking by use of MRI. Nat Clin Pract Cardiovasc Med. 2006; 3(10):554–562. [PubMed: 16990841]

8. Na HB, Song IC, Hyeon T. Inorganic Nanoparticles for MRI Contrast Agents. Adv Mater. 2009; 21(21):2133–2148.
9. (a) Nkansah MK, Thakral D, Shapiro EM. Magnetic poly(lactide-co-glycolide) and cellulose particles for MRI-based cell tracking. Magn Reson Med. 2011; 65(6):1776–85. [PubMed: 21404328] (b) Guzman R, Uchida N, Bliss TM, He D, Christopherson KK, Stellwagen D, Capela A, Greve J, Malenka RC, Moseley ME, Palmer TD, Steinberg GK. Long-term monitoring of transplanted human neural stem cells in developmental and pathological contexts with MRI. Proc Natl Acad Sci U S A. 2007; 104(24):10211–6. [PubMed: 17553967] (c) Lee ESM, Chan J, Shuter B, Tan LG, Chong MSK, Ramachandra DL, Dawe GS, Ding J, Teoh SH, Beuf O, Briguet A, Chiu Tam K, Choolani M, Wang S-C. Microgel Iron Oxide Nanoparticles for Tracking Human Fetal Mesenchymal Stem Cells Through Magnetic Resonance Imaging. Stem Cells. 2009; 27(8):1921–1931. [PubMed: 19544438]
10. Panyam J, Labhasetwar V. Dynamics of endocytosis and exocytosis of poly(D,L-lactide-co-glycolide) nanoparticles in vascular smooth muscle cells. Pharm Res. 2003; 20(2):212–20. [PubMed: 12636159]
11. Chithrani BD, Chan WCW. Elucidating the Mechanism of Cellular Uptake and Removal of Protein-Coated Gold Nanoparticles of Different Sizes and Shapes. Nano Lett. 2007; 7(6):1542–1550. [PubMed: 17465586]
12. Sarkar D, Ankrum JA, Teo GSL, Carman CV, Karp JM. Cellular and extracellular programming of cell fate through engineered intracrine-, paracrine-, and endocrine-like mechanisms. Biomaterials. 2011; 32(11):3053–3061. [PubMed: 21262537]
13. Xu CJ, Sun S. Superparamagnetic nanoparticles as targeted probes for diagnostic and therapeutic applications. Dalton Trans. 2009; (29):5583–591. [PubMed: 20449070]
14. Wang YX, Hussain SM, Krestin GP. Superparamagnetic iron oxide contrast agents: physicochemical characteristics and applications in MR imaging. Eur Radiol. 2001; 11(11):2319–31. [PubMed: 11702180]
15. (a) Cheng FY, Wang SP, Su CH, Tsai TL, Wu PC, Shieh DB, Chen JH, Hsieh PC, Yeh CS. Stabilizer-free poly(lactide-co-glycolide) nanoparticles for multimodal biomedical probes. Biomaterials. 2008; 29(13):2104–12. [PubMed: 18276001] (b) Brown KA, Vassiliou CC, Issadore D, Berezovsky J, Cima MJ, Westervelt RM. Scaling of transverse nuclear magnetic relaxation due to magnetic nanoparticle aggregation. J Magn Magn Mater. 2010; 322(20):3122–3126. [PubMed: 20689678]
16. Mailander V, Landfester K. Interaction of Nanoparticles with Cells. Biomacromolecules. 2009; 10(9):2379–2400. [PubMed: 19637907]
17. Lee N, Kim H, Choi SH, Park M, Kim D, Kim HC, Choi Y, Lin S, Kim BH, Jung HS, Kim H, Park KS, Moon WK, Hyeon T. Magnetosome-like ferrimagnetic iron oxide nanocubes for highly sensitive MRI of single cells and transplanted pancreatic islets. Proc Natl Acad Sci U S A. 2011; 108(7):2662–2667. [PubMed: 21282616]
18. Soenen SJ, Himmelreich U, Nuytten N, Pisanic TR 2nd, Ferrari A, De Cuyper M. Intracellular nanoparticle coating stability determines nanoparticle diagnostics efficacy and cell functionality. Small. 2010; 6(19):2136–45. [PubMed: 20818621]
19. Chung TH, Hsiao JK, Hsu SC, Yao M, Chen YC, Wang SW, Kuo MYP, Yang CS, Huang DM. Iron Oxide Nanoparticle-Induced Epidermal Growth Factor Receptor Expression in Human Stem Cells for Tumor Therapy. ACS Nano. 2011; 5(12):9807–9816. [PubMed: 22053840]
20. Chamberlain G, Smith H, Rainger GE, Middleton J. Mesenchymal stem cells exhibit firm adhesion, crawling, spreading and transmigration across aortic endothelial cells: effects of chemokines and shear. PLoS One. 2011; 6(9):e25663. [PubMed: 21980522]
21. Sarkar D, Spencer JA, Phillips JA, Zhao W, Schafer S, Spelke DP, Mortensen LJ, Ruiz JP, Vemula PK, Sridharan R, Kumar S, Karnik R, Lin CP, Karp JM. Engineered cell homing. Blood. 2011; 118(25):e184–e191. [PubMed: 22034631]
22. Colter DC, Class R, DiGirolamo CM, Prockop DJ. Rapid expansion of recycling stem cells in cultures of plastic-adherent cells from human bone marrow. Proc Natl Acad Sci U S A. 2000; 97(7):3213–8. [PubMed: 10725391]

23. Veilleux I, Spencer JA, Biss DP, Cote D, Lin CP. In vivo cell tracking with video rate multimodality laser scanning microscopy. IEEE J Sel Top Quantum Electron. 2008; 14(1):10–18.

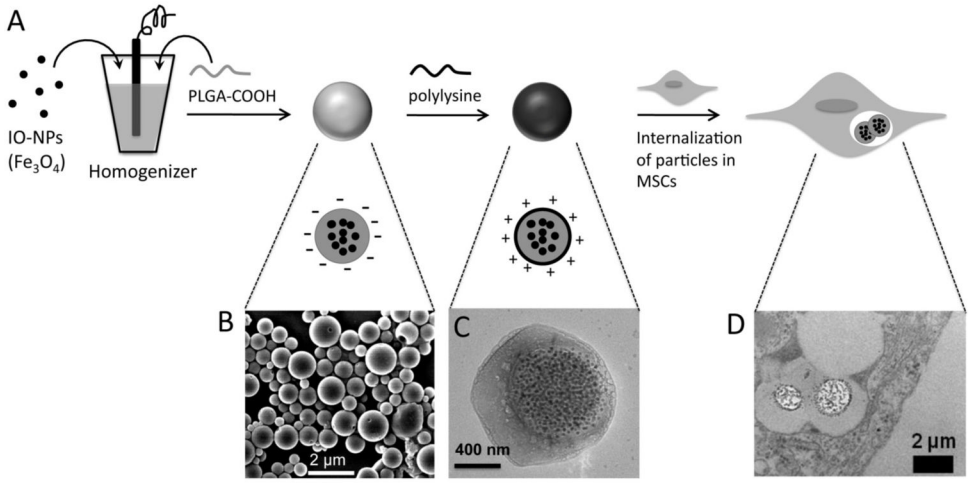

Figure 1.

IO:PLGA-MPs preparation and internalization by MSCs: (**A**) Schematic illustration of the preparation of IO:PLGA-MPs with single emulsion method. (**B**) SEM image of IO:PLGA-MPs. (**C**) TEM image of a representative IO:PLGA-MP. (**D**) TEM image of IO:PLGA-MPs internalized in a MSC.

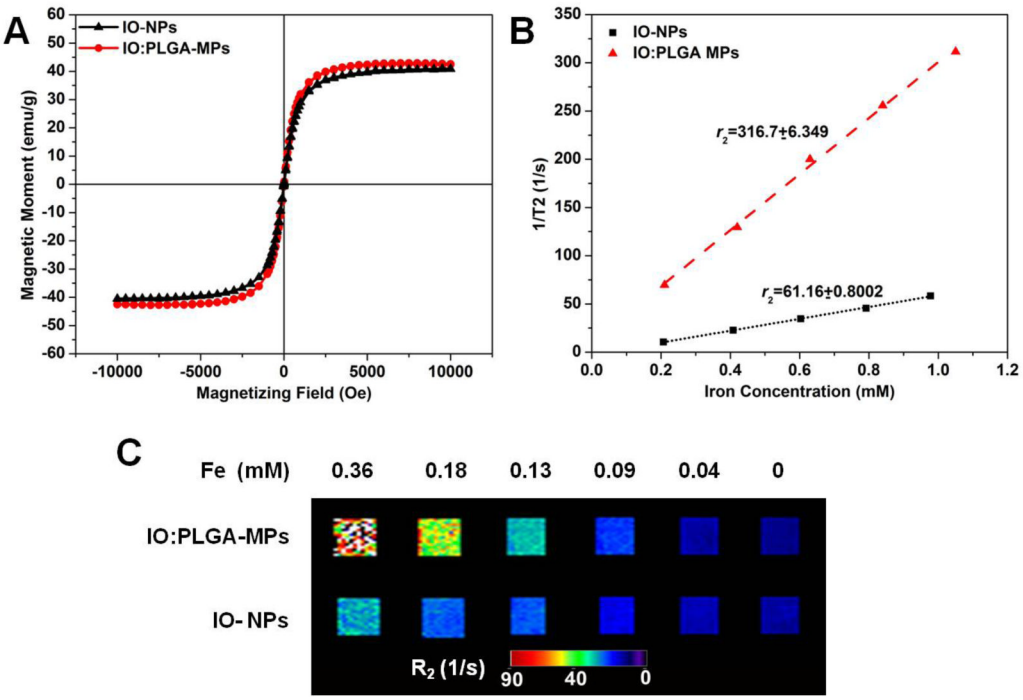

Figure 2.

Characterization of magnetic properties of particles prior to cellular internalization: (**A**) Hysteresis loop and (**B**) $1/T_2$ versus iron concentration for IO-NPs and IO:PLGA-MPs measured at 300 K. Relaxivity values r_2 were obtained from the slope of the linear fit of the experimental data. (**C**) R_2-weighted MRI images of 3% agarose gels containing IO-NPs and IO:PLGA-MPs at iron concentrations of 0, 0.04, 0.09, 0.13, 0.18, and 0.36mM. Pseudocolor was applied to reveal the R_2 value (unit: Hz or 1/s), as indicated by the scale bar.

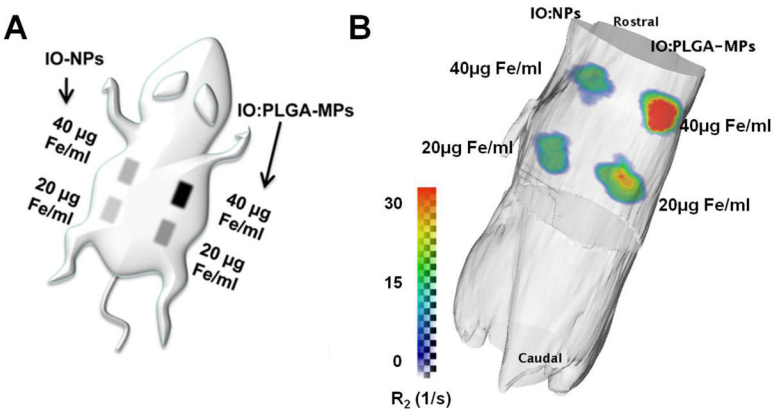

Figure 3.

Improved R2 contrast enhancement *in vivo* after PLGA encapsulation: **A**) Schematic illustration of the subcutaneous injection of 45 μL 3% agarose suspension of either IO-NPs (left) or IO:PLGA-MPs (right) or at the iron concentration of 20 μg Fe/ml (0.36mM) and 40 μg Fe/ml (0.71mM) on the back of the mouse. **B**) 3D reconstruction of a mouse with the R2 map collected with a 4.7 T Bruker Pharmascan scanner and calculated within the Osirix environment. Scale bar indicates the value of R2 (unit: 1/s or Hz).

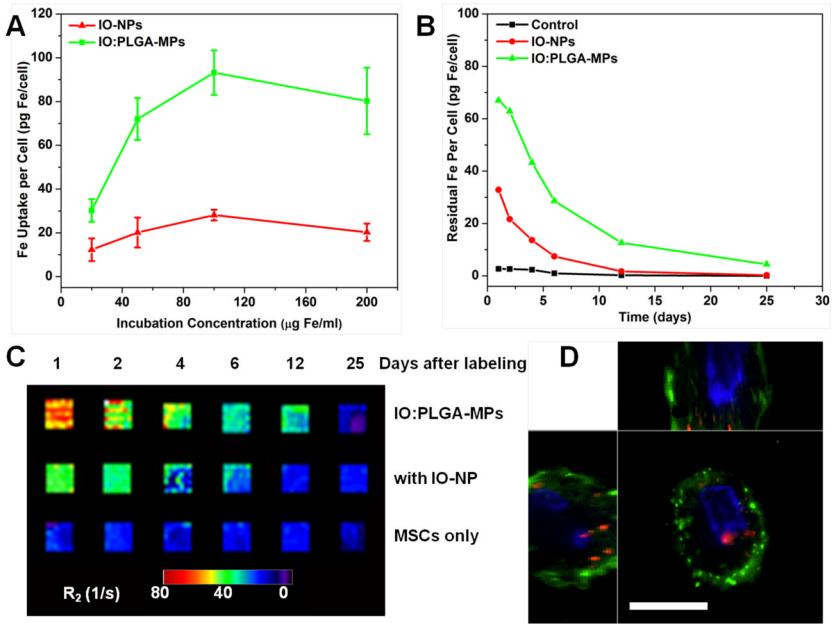

Figure 4.

Improved retention of IO in MSCs after PLGA encapsulation: (**A**) Cellular Fe content of MSCs after incubation with magnetic particles as a function of iron concentration. (**B**) Change in cellular iron content per cell after initial labeling with IO-NPs or IO:PLGA-MPs at the incubation concentration of 50μg Fe/ml. (**C**) R_2-weighted MR images of 200,000 MSCs collected at different time points and suspended in 3% agarose gels (4×4 mm^2 per square). (D) Fluorescent confocal image of MSCs 18 days after labeling with IO:PLGA-MPs. The plasma membrane is stained green (DiO), the nucleus is blue (DAPI) and the IO:PLGA-MPs are stained red (DiI). Scale bar is 10μm.

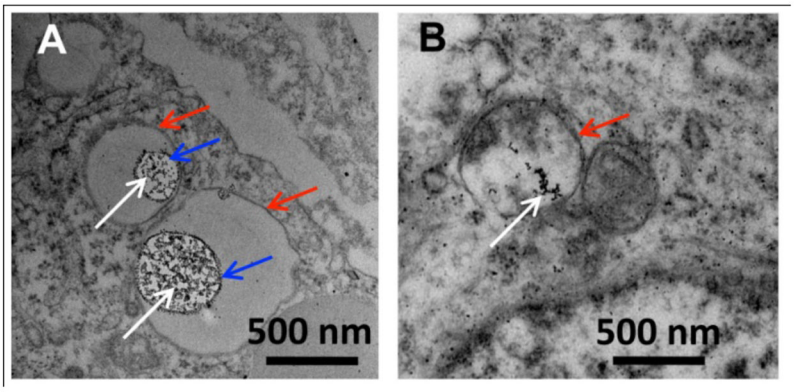

Figure 5.
TEM images of MSCs after 12 hours labeling with (**A**) IO:PLGA-MPs and (**B**) IO-NPs. White arrow: location of IO-NPs, Blue arrow: PLGA-MPs, Red arrow: membrane of intracellular compartment. The small size of the PLGA particles identified in TEM images suggests that the PLGA partially dissolved during TEM processing.

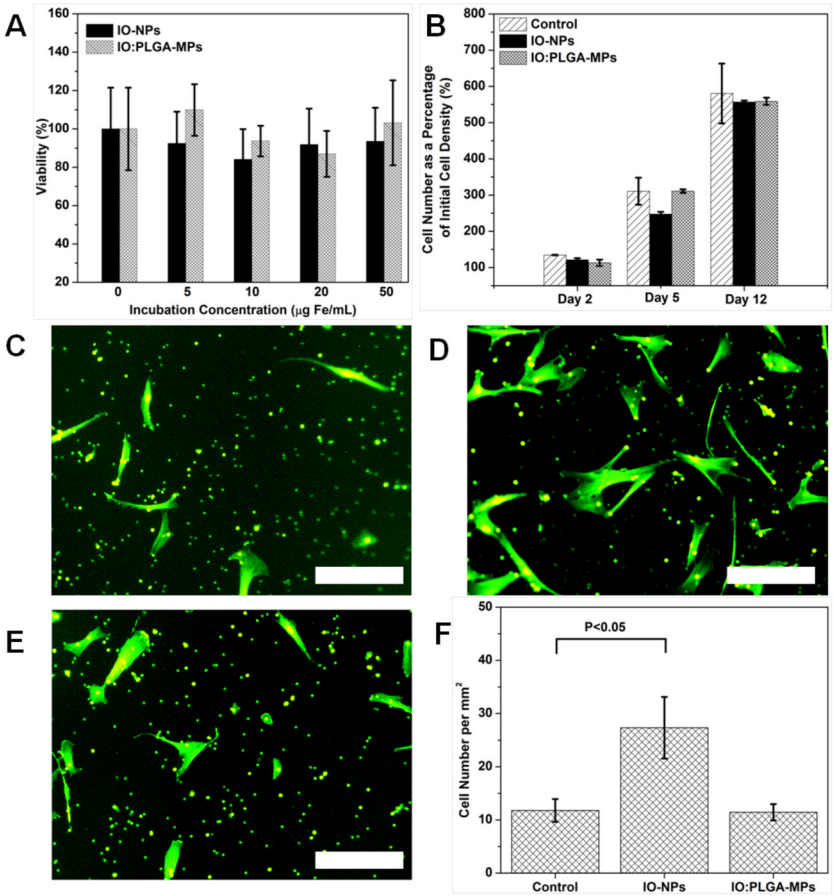

Figure 6.

Impact of particle labeling on cell viability, migration and proliferation. (**A**) Viability of iron-labeled MSCs as a function of iron concentration during the incubation. (**B**) Proliferation of MSCs labeled with magnetic particles. (**C–E**) Representative images of migrated MSCs through FluoroBlok™ 8.0 μm colored PET membrane (images acquired of Phalloidin-FITC stained cells shown as green from underside of membranes). (**C**) Unmodified control MSCs, (**D**) MSCs labeled with IO-NPs, (**C**) MSCs labeled with IO:PLGA-MPs. (**F**) Quantification of migrated MSCs (each experiment was repeated 3 times). Scale bar is 200 μm.

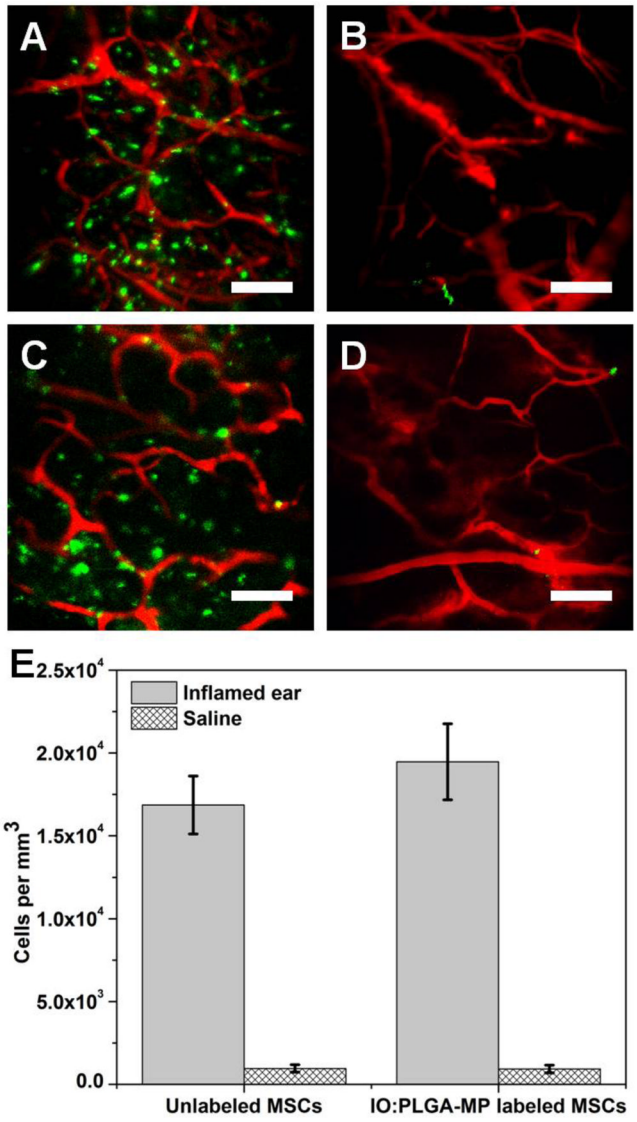

Figure 7.

(**A–B**) Representative images of homed unlabeled MSCs and (**C-D**) MSCs prelabeled with IO:PLGA-MPs in the (**A,C**) LPS ears and (**B,D**) saline ears. Green signal indicates MSCs and red signal is from the blood vessels perfused with FITC-Dextran, Bar = 100 μm. (**E**) Quantification of the MSCs in LPS and saline ears (each experiment was repeated 3 times).